ANALYSING DEFECTS IN SILICON BY TEMPERATURE- AND INJECTION-DEPENDENT LIFETIME SPECTROSCOPY (*T*-IDLS)

S. Diez, S. Rein and S.W. Glunz
Fraunhofer Institute for Solar Energy Systems ISE, Heidenhofstr. 2, D-79110 Freiburg, Germany
Phone ++49 761-4588-5271; Fax ++49 761-4588-9250, email: stephan.diez@ise.fraunhofer.de

ABSTRACT: To demonstrate the full potential of temperature- and injection-dependent lifetime spectroscopy (*T*-IDLS) as a method to characterise defects in silicon, measurements on an intentionally tungsten-contaminated wafer were performed at different temperatures up to 151 °C. By determination of the recently introduced defect parameter solution surface (DPSS) the detailed analysis revealed two discrete solutions regarding a deep defect level. Due to high accuracy of the measurements and due to a temperature range that allowed the turnover from increasing to decreasing lifetime to be observed, identification of a unique solution of the defect parameters has been achieved. These findings precisely confirm recent predictions in a theoretical study. Thus, the energy level and band gap half of the underlying deep defect related to tungsten could be determined unambiguously: E_t-E_V=0.34±0.02 eV with a corresponding ratio of capture cross-section asymmetry k=σ_n/σ_p=9.6±4. An investigation of the temperature dependence of the minority carrier capture cross-section identified the multiphonon emission capture as the relevant mechanism underlying recombination. The activation energy is determined as E_∞=0.017±0.003 eV.

Keywords: Lifetime, Spectroscopy, Defects, Tungsten.

1. INTRODUCTION

Since material quality has a strong influence on the efficiency of solar cells, it is an important task to analyse recombination-active defects introduced during crystal growth and the solar cell process. Lifetime spectroscopy (LS) is a highly sensitive diagnostic tool to detect and identify impurities and defects in semiconductors like silicon. Compared to the well-established deep-level transient spectroscopy (DLTS), LS is particularly useful to analyse recombination-active defects, i.e. those affecting device performance.

Usually only a broad range of defect energy levels E_t results from injection-dependent lifetime spectroscopy (IDLS) on one sample at room temperature [1]. The standard temperature-dependent lifetime spectroscopy (TDLS) is capable to determine this energy depth but assumes temperature-independent capture cross-sections for electrons σ_n and holes σ_p. Advanced TDLS overcomes this limitation by more sophisticated evaluation and modelling and allows for an increased spectroscopic information. Combining the results of TDLS and room-temperature IDLS makes it possible to determine the defect energy level E_t and the ratio k:=σ_n/σ_p [2, 3].

Within a theoretical study in Ref. [3], it is shown that increasing the information on the injection and temperature dependence by measuring injection-dependent lifetime curves at various temperatures should yield unambiguous spectroscopic results. Temperature- and injection-dependent lifetime spectroscopy (*T*-IDLS) was performed with a single experimental setup based on an apparatus intended for quasi-steady-state photoconductance (QSSPC) measurements. However, modelling of lifetime curves only resulted in a broad energy interval (0.45 – 0.9 eV below E_C) and thus did not allow the dominant defect level to be identified unambiguously [4]. The most likely reason is that the covered temperature range was too small for the investigated defect to observe the turnover of the lifetime curves from an increasing to a decreasing shape. Another *T*-IDLS investigation reached this turnover point. Nevertheless, a detailed analysis of these experimental data resulted in two discrete solutions for the parameters of the investigated molybdenum defect [5]. As this experiment was performed by means of the microwave-detected photo conductance decay technique (MW-PCD), it faced the problem of an extended data preparation and measurement time.

2. EXPERIMENTAL PROCEDURE AND RESULTS

In this study, we performed *T*-IDLS-measurements on an intentionally tungsten-contaminated *p*-type silicon sample based on the well-established setup for QSSPC-technique with a photographic flash lamp [6]. The sample was heated by a resistive element by means of a brass coil placed directly on top of the sample. The latter is built up from a system supplied by Sinton Consulting that was slightly modified. Thermal isolation via a pyrex sample underlay kept at a small distance from the measurement coil is adequate not to alter the calibration (voltage signal against conductivity) of the system by heating of the sample in the investigated temperature range. A Pt100-sensor measured the temperature on top of the sample.

Adding tungsten to the silicon melt before pulling a mono-crystalline Cz-Si-crystal resulted in intentional contamination. An acidic etch removed the crystal damage of the wafers. The doping concentration of the sample discussed in this paper (N_A=4.1x10^{14} cm^{-3}) was determined by resistance measurements based on the four-point probe technique. It is roughly two to three orders of magnitude higher than the concentration of tungsten specified by the calculation from the manufacturer based on the segregation coefficient. For the determination of the carrier lifetime, the samples were passivated with a high-quality silicon nitride [3] exhibiting surface recombination velocities as low as 10 cm/s. This was confirmed by reference samples without metal contamination. Thus, after correcting for

Auger- and radiative recombination [7] that affected only a small range at the highest injection level beyond an injection density of Δn=1×10^{16} cm^{-3}, the resulting effective lifetime can be attributed to bulk defects. These injection-dependent lifetime curves are shown in Fig. 1 for temperatures up to 151 °C. Remeasuring the lifetime after this temperature raise yielded values coinciding with the initial curve at room temperature. This argues for unchanged defect structures.

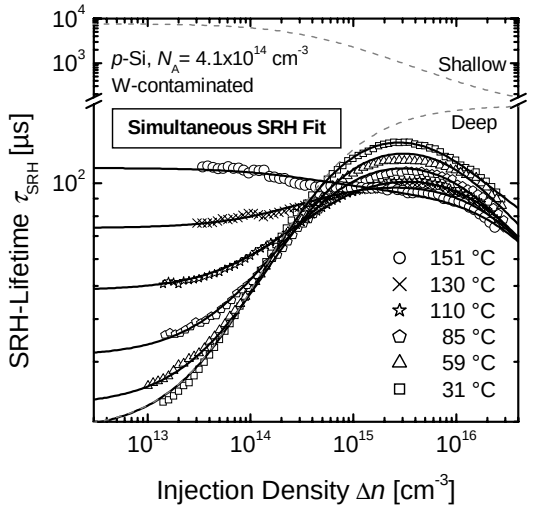

Fig. 1 Injection dependence of the effective SRH carrier lifetime measured on a W-contaminated sample after subtracting the little influence of intrinsic recombination beyond Δn=1×10^{16} cm^{-3}. A change from increasing to decreasing shape is observed by covering the range from room temperature up to 151 °C. Solid lines display a simultaneous fit with a single unique set of parameters for a deep (E_t-E_V=0.34 eV, symmetry factor k=9.6) and a shallow defect (E_C-E_t=0.17 eV, k=3.4). They result from a detailed DPSS analysis. Separately plotting SRH lifetime for these defects at 31 °C (dashed curves) reveals the sole dominance of the former up to beyond Δn=1×10^{15} cm^{-3}. It is attributed to a tungsten-related bulk defect.

3. EVALUATION OF MEASUREMENTS

Sample heating caused a temperature difference regarding the reference cell kept at room temperature. This effect can be neglected with respect to determination of the carrier generation rate attributed to the wafer. In contrast, the sensitivity of the carrier mobility on temperature for calculating the injection level Δn from conductivity measurements has to be taken into account. For this purpose, the mobility model by Dorkel and Leturcq was chosen [8].

Investigations of the lifetime curves to extract as much information as possible to characterise underlying defects were performed by determination of the Defect Parameter Solution Surface (DPSS) which visualises the ambiguity of fit results of a single lifetime curve [3, 5]. The recombination lifetime attributed to a single defect was modelled by the standard SRH-theory [9]:

$$\tau_{SRH} = \tau_{n0}\frac{(p_0 + p_1 + \Delta n) + k(n_0 + n_1 + \Delta n)}{p_0 + n_0 + \Delta n} \qquad (1)$$

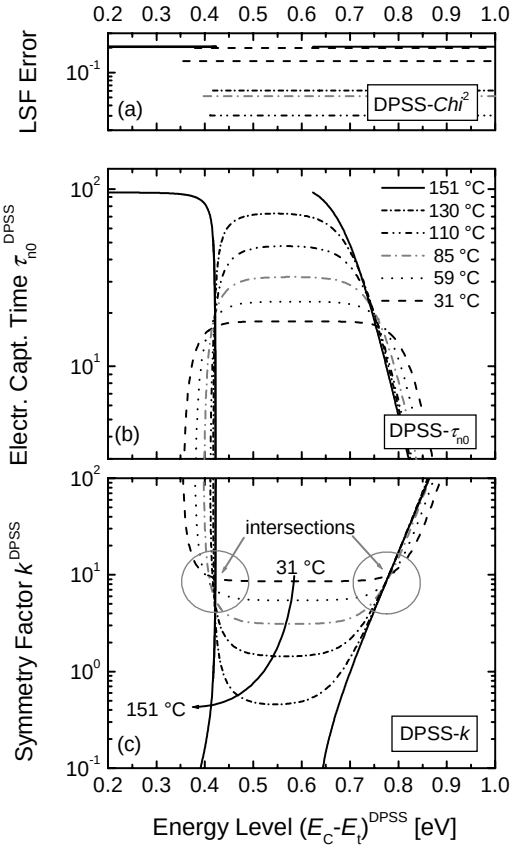

Fig. 2 DPSS analysis of *T*-IDLS curves measured at different temperatures. Parameters for a shallow defect (E_C-E_t=0.17 eV, k=4.3) gained from an initial simultaneous two-defect fit with standard SRH- modelling were fixed. The energy level $(E_C\text{-}E_t)^{DPSS}$ attributed to a necessary second defect was specified but gradually varied. The resulting parameter combinations, i.e. one k^{DPSS} and one τ_{n0}^{DPSS} curve calculated for each temperature separately, are superposed in Fig. 2c and *b* respectively. The plot of the Chi^2-results in Fig. 2a assesses the quality of least squares fitting and reveals gaps (see solid lines, 151 °C) corresponding to nonexistent parameters for appropriate modelling of the curves within the corresponding $(E_C\text{-}E_t)^{DPSS}$ range.

where n_0 and p_0 are the equilibrium densities of electrons and holes, respectively, n_1=N_C×exp[-(E_C-E_t)/k_BT] and p_1=N_V×exp[-(E_t-E_V)/k_BT] the so-called SRH densities depending on the energy level E_t of the recombination center. The inverse product of the defect concentration N_t, thermal velocity v_{th} and σ_n equals the electron capture time constant τ_{n0} acting as a scaling factor in Eq. (1):

$$\tau_{n0} := \left(N_t \sigma_n v_{th}\right)^{-1} \qquad (2)$$

Initially, an adequate simultaneous least squares fit involving all lifetime curves was achieved by accounting for a deep and a shallow defect. Parameters determining the SRH lifetime corresponding to the shallow defect were obtained (E_C-E_t=0.17 eV, k=4.3). Keeping these parameters of the shallow defect fixed for the following analysis a sequence of least squares optimisation fitting the deep level for a certain energy level $(E_C\text{-}E_t)^{DPSS}$ was separately performed for each of the *T*-IDLS-curves. The

arising triple of curves made up of error Chi^2, optimal symmetry factor k^{DPSS} and $\tau_{n0}{}^{DPSS}$ values describing this second defect are visualised in the DPSS diagram shown in Figs. 2a-c as a function of the DPSS defect energy level $(E_C\text{-}E_t)^{DPSS}$. For each temperature, these three curves represent all possible SRH parameterisations which are equal with respect to similar quality of the modelling for the considered temperature. As can be seen from truncated DPSS-Chi^2 curves their range of validity is limited. The fact that the fit quality for a specified temperature is identical for a broad range of $(E_C\text{-}E_t)^{DPSS}$ values visualises the strong ambiguity of the SRH parameterisation of a single IDLS curve as discussed in detail in [3].

The qualitative change of the underlying lifetime curves from increasing to decreasing shape below around Δn=3x10^{15} cm^{-3} due to heating of the sample corresponds to a qualitative change of the curves within the DPSS plots of Fig. 2. This is exemplified by the arrow in Fig. 2c. Deep defect levels are more recombination-active under low- compared to high-level injection according to Eq. (1). Thus, decreasing lifetime curves at higher temperatures like the plot for 151 °C in Fig. 1 embody specific characteristics in the DPSS plots of Fig. 2: a split range of validity with a gap around mid gap (break in solid curve in Fig. 2a).

4. DISCUSSION

The true defect parameters should result from a common intersection point of all DPSS-*k* curves. Their superposition in Fig. 2c reveals two intersection points though. Proximate values are plotted together with corresponding DPSS-τ_{n0} curves in more detail in Figs. 3c and b respectively. Thus two parameter sets are valid at first glance.

However, applying a similar DPSS analysis to lifetime curves simulated with Eq. (1) instead of measured data reveals the difference in the two intersections of the DPSS-*k* curves. Thereby, the true parameters chosen for the simulation of the investigated lifetime data correspond to a sharp intersection point. The second intersection point is more diffuse if decreasing lifetime curves are included in addition to increasing ones. This effect has been quantified theoretically in [3]. To extract the true solution by the sharpness of the intersection points thus requires both types of qualitatively different lifetime curves (raising and falling) to be included in the analysis.

In order to distinguish between the two intersection points associated with the DPSS analysis of the W-contaminated sample DPSS-*k* values at specified DPSS energies were averaged and the relative standard deviation $\Delta_{rel}[k]$ was computed. The $\Delta_{rel}[k]$ values in vicinity of the two minima are exhibited in Fig. 3a. As a measure of uncertainty of the desired parameters values corresponding to three times the minimal standard deviations were tolerated and marked by shaded areas. The resulting discrete levels with the approximate errors are $E_C\text{-}E_t$=0.42±0.005 eV for the first minimum located in the upper band gap half and $E_t\text{-}E_V$=0.34±0.02 eV corresponding to k=9.6±4 for the second minimum in the lower band gap half respectively. As expected due to the above mentioned lifetime simulation analysis the DPSS-*k* curve corresponding to a

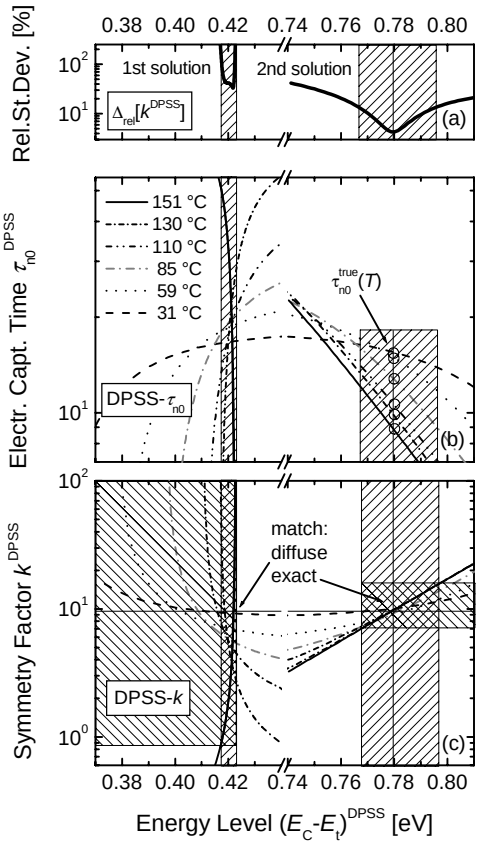

Fig. 3 DPSS analysis of a W-contaminated sample corresponding to *T*-IDLS curves measured at different temperatures. DPSS-*k* values at specified DPSS energies were averaged. The corresponding standard deviation $\Delta_{rel}[k]$ is shown in Fig 3a. The DPSS-*k* and DPSS-τ_{n0} curves shown in Fig 3b and *c* correspond to a more detailed plot of the values shown in Fig. 2b and c respectively in the vicinity of the two minima revealed by the $\Delta_{rel}[k]$ plot. The latter reflect the optimum energy positions for the intersection points and allow the true defect parameters (2nd solution: $E_t\text{-}E_V$=0.34±0.02 eV and k=9.6±4) to be identified by the sharpness of the intersection points of the DPSS-*k* curves. Shaded areas represent an error estimation by tolerating parameters corresponding to three times the minimal standard deviations.

temperature of 151 °C causes one intersection point to be more diffuse. This becomes manifest in Fig. 3a by a minimum standard deviation of the first solution that is about one order of magnitude larger (more diffuse intersection) than for the second sharp intersection point. Further, this DPSS-*k* curve induces an estimated error of the corresponding *k* value covering a range of about two orders of magnitude. Thus the two solutions are not equivalent and the second intersection can be identified with the true defect parameters.

Together with the above mentioned characteristics describing the shallow defect, the unique unambiguous parameters of the second intersection point of the DPSS-*k* curves for the deep energy level resulted in a simultaneous modelling of high accuracy of the whole set of *T*-IDLS curves. This result of the detailed DPSS analysis is shown in Fig. 1 by the solid lines.

Due to the temperature dependence of the electron capture time constant τ_{n0}, a common intersection point of all DPPS-τ_{n0} curves at the true defect energy level can not be expected. This is confirmed by looking at the intersection of the line marking the true energy value at E_t-E_V=0.34 eV with the DPSS-τ_{n0} curves in Fig. 3b. Nevertheless, the τ_{n0} values for different temperatures at this constant energy (see circles in Fig. 3b contain information about the temperature dependence of the capture cross-section for electrons, $\sigma_n(T)$, as suggested by Eq (2). Fig. 4 shows the resultant product of the electron capture cross-section $\sigma_n(T)$ and the defect concentration in a logarithmic plot versus the inverse temperature.

A linear correlation can be identified indicated by the straight line. This result can provide insight into the underlying mechanism of recombination as it is characteristic for multiphonon emission causing an efficient capture process [10]. This model attributes electron capture to lattice vibrations which cause the crossing of the defect energy level into the conduction band. The need of sufficiently large vibrations of the defect on its lattice site to initiate transition between the free carrier and the bound carrier levels (vibronic coupling) result in the investigated increase of capture probability and thus a decrease in τ_{n0} with increasing temperature. The model comprises a thermally activated cross-section whereas a free electron in the conduction band has to overcome a thermal barrier to be captured by the defect:

$$\sigma(T) = \sigma_\infty \times \exp\left(-\frac{E_\infty}{kT}\right) \qquad (3)$$

A linear fit to the data in Fig. 4 yields an activation energy of E_∞=0.017±0.003 eV.

Especially in earlier literature several deep energy levels have been observed in silicon contaminated with tungsten. More recently, it was supposed that several of them could probably be explained by a high chemical reactivity of interstitial tungsten and additional unwanted impurities and only a single donor level in the lower band gap half due to an interstitial defect was suggested. This corresponds to the chemical trend within the chromium group exhibiting only one donor state what is well established for Cr and Mo [11]. The results above confirm this suggestion as Fig. 1 approves that just one relative deep level located in the lower band gap half is needed to achieve an accurate modelling of the lifetime data up to medium injection levels. The resulting energy depth of E_t-E_V=0.34 eV is within a range covered by results in the literature between 0.33 eV [12] and 0.40 eV [11] above the valence band.

By using the value of the hole capture cross-section in the literature [11], σ_p=5.0×10^{-16} cm^2, the above-determined capture asymmetry factor, k=9.6, and hereby σ_n=σ_p×k=4.8×10^{-15} cm^2, allows the defect concentration to be estimated by the use of Eq. (2) which is around N_t=1.4×10^{-12} cm^{-3}.

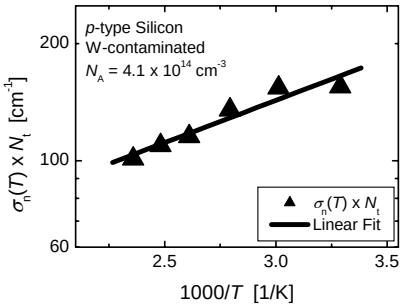

Fig. 4 Temperature dependence of the capture cross-section for electrons, σ_n. The data corresponds to the true $\tau_{n0}(T)$ values (see circles in Fig. 3b of the different temperatures investigated by lifetime measurements at the energy level E_t-E_V=0.34 eV determined by the detailed DPSS analysis that is attributed to a tungsten-related deep defect. The fit shows the linear correlation that is characteristic of a capture process attributed to multiphonon emission.

5. CONCLUSION

The detailed DPSS study of a tungsten-contaminated *p*-type silicon wafer by means of *T*-IDLS clearly shows the capability of this method, to overcome the large ambiguousness of a single injection-dependent measurement (IDLS). In accordance with theoretical investigations two discrete solutions for the desired defect parameters were found whereas the mandatory accuracy of the experiment enabled the extraction of the true solution by its sharp intersection point in the DPSS-*k* graph. Thus, the energy level and band gap half of the underlying W-related defect with a relatively deep energy level could be determined in accordance with the spectrum of values found in the literature: E_t-E_V=0.34±0.02 eV. In addition, the ratio k=σ_n/σ_p=9.6±4 was obtained. An investigation of the temperature dependence of the capture cross-section for electrons enables the identification of the underlying recombination process to be driven by multiphonon emission with an activation energy of E_∞=0.017±0.003 eV.

ACKNOWLEDGEMENTS

The authors would like to thank M. Kwiatkowska, C. Baur and J. Holtkamp for their support as well as Prof. T. Abe (ShinEtsu) for supplying the investigated wafers.

REFERENCES

[1] S. Rein and S. W. Glunz, *Proc. 19th EU PVSEC* (Paris, France 2004) p. 479-83.
[2] S. Rein and S. W. Glunz, Appl. Phys. Lett. 82 (2003) p. 1054-56.
[3] S. Rein, Lifetime Spectroscopy - A Method of Defect Characterization in Silicon for Photovoltaic Applications (Springer, Berlin-Heidelberg, 2005).
[4] J. Schmidt and R. A. Sinton, *Proc. 3rd WC PVEC* (Osaka, Japan, 2003) p. 947-50.
[5] S. Rein, S. Diez, and S. W. Glunz, *Proc. 19th EU PVSEC* (Paris, France, 2004) p. 219-22.
[6] R. A. Sinton, A. Cuevas, and M. Stuckings, *Proc. 25th IEEE PVSC* (New York, NY, USA 1996) p. 457-60.
[7] M.J. Kerr, PhD thesis, Australian National University (2002).
[8] J. M. Dorkel and P. Leturcq, Solid-State Electron. 24 (1981) p. 821-25.
[9] W. Shockley and W. T. J. Read, Phys. Rev. 87 (1952) p. 835-42+.
[10] C. H. Henry and D. V. Lang, Physical Review B (Solid State) 15 (1977) p. 989-1016.
[11] K. Graff, Metal Impurities in Silicon-Device Fabrication, 1st ed. (Springer-Verlag, Berlin, 1995).
[12] S. Boughaba and D. Mathiot, J. Appl. Phys. 69 (1991) p. 278-83.